

Quantum coherence in the dynamical excitation, ionization, and decaying of neon gas induced by X-ray laser

Yongqiang Li¹, Cheng Gao¹, Wenpu Dong¹, Jiaolong Zeng¹ and Jianmin Yuan^{1,2}

¹*Department of Physics, National University of Defense Technology, Changsha 410073, P. R. China*

²*IFSA Collaborative Innovation Center, Shanghai Jiao Tong University, Shanghai 200240, P. R. China**

(Dated: January 13, 2015)

We develop a large scale quantum master equation approach to describe dynamical processes of practical open quantum systems driven by both coherent and stochastic interactions by including more than one thousand true states of the systems, motivated by the development of highly bright and fully coherent lasers in the X-ray wavelength regime. The method combines the processes of coherent dynamics induced by the X-ray laser and incoherent relaxations due to spontaneous emissions, Auger decays, and electronic collisions. As examples, theoretical investigation of *real* coherent dynamics of inner-shell electrons of a neon gas, irradiated by a high-intensity X-ray laser with a full temporal coherence, is carried out with the approach. In contrast to the rate equation treatment, we find that coherence can suppress the multiphoton absorptions of a neon gas in the ultra-intense X-ray pulse, due to coherence-induced Rabi oscillations and power broadening effects. We study the influence of coherence on ionization processes of neon, and directly prove that sequential single-photon processes for both outer- and inner-shell electrons dominate the ionizations for the recently typical experiments with a laser intensity of $\approx 10^{18}$ W/cm². We discuss possible experimental implementations such as signatures for coherent evolution of inner-shell electrons via resonance fluorescence processes. The approach can also be applied to many different practical open quantum systems in atomic, quantum optical, and cold matter systems, which are treated qualitatively by a few-level master equation model before.

PACS numbers: Subject Areas: Atomic and Molecular Physics, Optics, Computational Physics

I. INTRODUCTION

Master equation approach is a standard technique for open quantum systems [1] and a successful theory in descriptions of light-matter interactions, such as in condensed matter physics [2], chemistry and biology [3], quantum optics [4], and ultracold gases [5]. The master equation is quite general and encompasses various physical phenomena, as long as these phenomena share common physical mechanisms, i.e. the interplay between coherence and dissipation. Traditionally, these kinds of systems are treated within the framework of few-level models [5–7]. With the development of highly bright lasers [8], however, the few-level models lose the possibility for describing complex open systems, since energy here is deposited in a broad range and relaxes in a vast number of decay channels. In this case, new challenges appear for real dynamics of these complex systems, and a large-scale simulation is inevitable. Here, one open issue, related to coherence effects in dynamical processes of complex systems, is still unknown.

Coherence plays an important role in describing correlation properties of quantum matters and understanding quantum phenomena including lasing [9], Fano shape [10], superconductivity, superfluidity and Bose-Einstein condensate [11, 12], and novel phenomena arising from quantum optics [13] and attosecond physics [14].

To study these coherence-induced quantum features, dramatic success has also been achieved in preparing and controlling the coherent dominant systems with suppressed dissipations, such as electromagnetically induced transparency in quantum optics [15] and superfluid-Mott phase transition in condensed matter physics [16]. Recently, exploring coherence effects of complex systems has been arguably one of the most important topics in physics, inspired by generating X-ray laser with extremely high brightness and fully temporal coherence [8], such as the Linac Coherent Light Source (LCLS) [17], where one opened a new era of exploring the interaction of high-intensity X rays with complex systems on femtosecond (fs) timescales. Unfortunately, a typical feature of X-ray-matter interactions is the rapid decay processes, due to the vast relax channels. As a result, it is inevitable to investigate the interplay between coherence-induced effects and dissipations in X-ray-matter systems.

Here, the X-ray free electron laser, with an ultrashort pulse duration and a high peak brilliance, provides the possibility for the study of physical, chemical and biological properties which are never accessed experimentally before [18]. For example, a series of pioneer experiments [19–28] focus on understanding of X-ray-matter interactions, including nonlinear photoionizations, hole relaxations, Auger electron distributions, and X-ray emission spectrums in atoms, molecules and solid materials. To simulate these experiments, a semiclassical description of radiation-field coupled systems, Einstein's rate equation approach [29–31], has recently been extended to the regime of X-ray-matter interactions for gaining fundamental insight into the fast decayed systems, by in-

*Electronic address: jmyuan@nudt.edu.cn

cluding photoexcitation and ionization, electron impact excitation and ionization, Auger decay, and their reverse processes. In Einstein's rate equation model, all the absorption and emission processes are treated with transition probability and the coherence between different levels is neglected, which are good approximations for either incoherent light fields or dominant decay processes of the systemic coherence [32]. The agreement that one finds between theoretical predictions [31] and experiments [20] at relatively low atomic number densities, verifies the capability of the model to simulate X-ray-matter interactions. The physical reason is that the free-electron laser beam has limited temporal coherence with each pulse consisting of a random number of incoherent intensity spikes in a fs duration.

One big challenge, however, which has not been overcome yet, is the temporal coherence of X-ray free-electron laser generated from self-amplified spontaneous emissions from electron beams [33]. One goal of the X-ray free-electron laser is to enhance temporal coherence of the field, and the quest for improved X-ray sources, based on the free electron laser, is being tackled with several techniques [25, 34–41]. In fact, the new X-ray pulse with improved temporal coherence [41] is more suitable to locally deposit energy and prepare electronic states, study dynamical properties via photon correlation spectroscopy, and image biological specimens and long-rang orders in liquid and condensed matters [18]. Recently, one generates the first successful coherent free-electron laser radiation pulses in the soft X-ray regime, based on the seeding experiment [42], which experimentally provides the possibility for investigating the interplay between coherence and dissipation in X-ray-matter systems. Then the crucial issue, related to an X-ray laser with an improved temporal coherence, is how to model the ultrafast dynamics of the X-ray-matter systems and understand the underlying physics. To obtain a more precise description of dynamical mechanics, in general, we need a quantum mechanical tool for simulations of its time evolution, such as time-dependent Schrödinger equation. In contrast to the case of low- Z species in dilute gases [43–48], time-dependent Schrödinger equation for complex systems is difficult to tackle directly, due to electron-electron correlations, collision processes, and spontaneous and Auger decay processes. Approximations for the X-ray-matter systems are inevitable, such as master equation approach. In the master equation approach, one can include the important microscopic processes as much as possible and investigate the interplay between coherence and dissipations in the X-ray-matter systems. Instead of a few-level simulations [5–7, 49–53], one need to simulate *real* dynamics of the complex X-ray-matter systems based on large scale simulations, due to the vast decay channels induced by the intense X-ray laser. As far as we know, this problem is never explored in the framework of quantum master equation approach before, coherent dynamics of the complex systems is still unclear, and it is still an open issue whether new phenomena arise from coherence

effects in the ultrafast decayed systems.

These questions motivate our study in this paper to establish a general method for describing coherent dynamics of the X-ray-matter systems in the framework of master equation approach. In principle, master equation approach can deal with different kinds of dynamics of the intense X-ray-matter systems by including the microscopic processes due to photons, electrons and environments. In dilute atomic gases [20, 26], for example, one should include photoexcitations and ionizations, Auger and spontaneous decay processes, and their reverse processes. For dilute molecules [21], additional processes, such as photon dissociations, should be taken into account. For solid-dense warm and hot matters [27], electron impact excitations and ionizations play an important role, in addition to environmental screening effects [60]. Therefore, we develop a thousand state master equation for describing *real* dynamics of these complex systems induced by an X-ray laser, and discuss possible experimental implementations such as signatures for coherent evolution of inner-shell electrons. Our studies will provide the basis for understanding the coherence effects in X-ray absorption mechanisms at a fundamental level. Actually, if all the off diagonal elements of the density matrix are ignored, our method reduces to Einstein's rate equation approach, which is a semiclassical description for X-ray-matter interactions [29–31]. The present approach can be applied to many different practical open quantum systems, which are widely treated qualitatively before by a few-level master equation approach [49], such as those in atomic physics [50], quantum optics [51] and cold matter physics [5, 52].

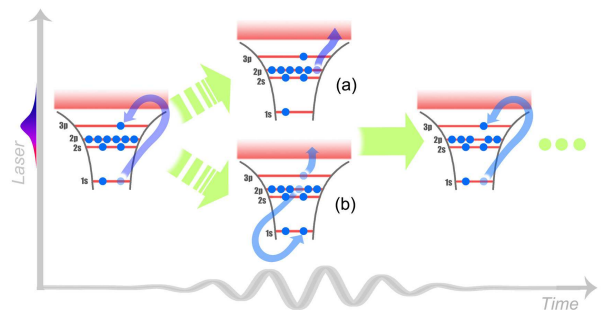


FIG. 1: Sketch of multiphoton absorptions in neon induced by ultra-intense X-ray pulses. Excitations and ionizations from the 1s shell dominate the photoabsorptions, followed by the consequent further outer-shell ionizations (a) and Auger decay processes (b), ending up with a highly ionized stage. Coherent Rabi oscillations interplay with dissipations in the X-ray-atom systems, such as Auger and spontaneous decay processes.

In the recently typical experiment [20], however, atomic gases are dilute and the influence of electron collisions and photon scattering can be neglected [30]. In this paper, we take dilute atomic gases as examples for discussing coherent dynamics of the rapidly decayed X-ray-matter systems (sketch in Fig. 1), where there are still few studies related to *real* dynamics of complex atoms

based on multilevel master equation approach [7]. Here, comparisons between master equation and rate equation approach will be made to investigate the influence of coherence on the dynamical mechanics, as related to the ongoing experiments with different temporal coherence. In parallel, we also perform an approximate calculation based on a degenerate atomic master equation approach which is computationally more affordable.

The paper is organized as follows: in section II we give a detailed description of the approach. Section III covers our results for coherent dynamics of neon induced by an X-ray laser, and discusses Auger processes of neon based on thousand state master equation approach. We summarize with a discussion in Section IV.

II. THEORETICAL MODEL

A. Hamiltonian

We consider a many-body system, such as dilute atomic and molecular gases [20, 21, 26], and solid-state materials [27], coupled with incoherent sources such as vacuum, irradiated by a high intensity X-ray laser. Inner-shell electrons of these atoms and molecules will be excited, forming a far-off-equilibrium system and typically relaxing in a fs timescale via spontaneous, Coulombic and Auger decay processes. These processes compete with other mechanics, such as processes including coherent photoexcitations and ionizations. Correspondingly, the total Hamiltonian of the X-ray-matter systems can be written as

$$\hat{H} = \hat{H}_A + \hat{H}_F + \hat{H}_I + \hat{H}_{\text{inc}}, \quad (1)$$

where the total Hamiltonian is the sum of the Hamiltonian \hat{H}_A of the many-body system in vacuum, the external field Hamiltonian \hat{H}_F including the coherent and incoherent external field, the laser-matter interaction \hat{H}_I , and the incoherent-field-matter interaction \hat{H}_{inc} .

The Hamiltonian

$$\hat{H}_A = \sum_{k=1}^N \epsilon_k \hat{A}_{kk}, \quad (2)$$

governs the time evolution of the system in vacuum, such as dilute atomic and molecular gases, and condensed materials, with $\hat{A}_{kk} = |k\rangle\langle k|$ and N being the total energy levels included. Here, $|k\rangle$ and ϵ_k denote the eigenstate and eigenvalue of the system, respectively. The Hamiltonian of the external field is given by

$$\hat{H}_F = \sum_i \hbar \omega_i^a \hat{a}_i^\dagger \hat{a}_i + \sum_i \hbar \omega_i^b \hat{b}_i^\dagger \hat{b}_i, \quad (3)$$

where \hbar denotes the reduced Planck constant, \hat{a}_i (\hat{a}_i^\dagger) denotes the annihilation (creation) operator that corresponds to the i -th mode of the laser with frequency ω_i^a , and \hat{b}_i and ω_i^b denote those for the incoherent field.

With the semi-classical treatment for the laser field, the quantization of the light is ignored. Instead the light is considered as a electric field, $E(t)$, which interacts with the i -th dipole \mathbf{d}_i for the transition between states $|k\rangle$ and $|k'\rangle$ to give

$$\hat{H}_I = - \sum_i \frac{\hbar \Omega_i(t)}{2} (\hat{D}_i e^{-i\omega_L t} + \text{H.c.}), \quad (4)$$

where the transition operator $\hat{D}_i = |k\rangle\langle k'|$, and Rabi frequency $\hbar \Omega_i(t) = e \mathbf{d}_i \cdot \mathbf{E}(t)$ at time t with $\mathbf{d}_i = \langle k' | \hat{\mathbf{d}}_i | k \rangle$. We remark here that we have used the dipole approximation for the coupling in Eq. (4), and can also trace out the external field degrees of freedom within the semi-classical treatment indicating the Eq. (3) can be ignored in the simulations. This semiclassical approximation forms the basis of most investigations on the many-body systems both coherently and incoherently coupled by a strong external field.

For magnetic sublevels, we rewrite the Hamiltonian of the matter-field interaction in a more explicit form

$$H_I = \sum_{J,J'} \frac{\hbar \Omega_i(t)}{2} (D_{JJ'\sigma} e^{-i\omega t} + \text{H.c.}), \quad (5)$$

where $\hbar \Omega_i(t) = e E(t) \langle J | \hat{\mathbf{d}}_i | J' \rangle$ and

$$D_{JJ'\sigma} = (-1)^{J-M_J} \begin{pmatrix} J & 1 & J' \\ -M_J & \sigma & M_J' \end{pmatrix} |J, m_J\rangle \langle J', m_J'|.$$

Here σ denotes the polarization of the external laser, and the dipole operator $\hat{\mathbf{d}}_i$ describes a $J \rightarrow J'$ transition between states $|J, M_J\rangle$ and $|J', M_J'\rangle$ with Zeeman substructures.

Actually, we can remove the explicit time dependence from the Hamiltonian, if Rabi frequency Ω is time independent and $\Omega \ll \epsilon_i, \omega$, transforming the Hamiltonian of the system to an arbitrarily specified rotating frame. The interaction Hamiltonian in a frame rotating at the laser frequency ω reads

$$H_I = \sum_{J,J'} \frac{\hbar \Omega}{2} (D_{JJ'\sigma} + \text{H.c.}). \quad (6)$$

The system can also be pumped by an incoherent field, such as the black-body radiation field in a hot plasma environment, and it reads

$$\hat{H}_{\text{inc}} = \hbar \sum_i \sum_n (\mathbf{d}_i \mathbf{e}_i \cdot \mathbf{e}_n \hat{b}_n \hat{D}_i + \text{H.c.}), \quad (7)$$

where \mathbf{e}_i and \mathbf{e}_n denote the directions of the dipole moment \mathbf{d}_i , the polarization of the incoherent field, respectively. Actually, the contributions of the incoherent field can directly be included in the master equation approach [6, 54], as discussed in Sec. II B.

B. Method

Now, the next question is how to theoretically simulate the time evolution of complex systems in the presence of the X-ray laser, described by Eq. (1). In contrast to low-Z atomic and molecular gases [43–48], the X-ray-matter system is dominated by ultrafast decayed mechanics in the experimental timescales, such as spontaneous decay processes, where one loses the possibility to keep track of the couplings between the system and the environment with infinite degrees of freedom. In solid-state materials, electron-ion, electron-electron and ion-ion collisions occur rapidly and randomly, where screening and broadening effects due to the solid-density environment should be taken into account in dynamical simulations. Hence, a statistical description for the X-ray-matter system is needed, and here we study the time evolution based on a generalized thousand state master equation approach for the reduced density matrix of the system, where the degrees of freedom of both the environment and X-ray laser have been traced out in a perturbative treatment. The generalized thousand-level master equation for a complex system, coupled to vacuum modes of the electromagnetic field and irradiated by an X-ray laser and incoherent radiation field, reads

$$\frac{d\hat{\rho}(t)}{dt} = -\frac{i}{\hbar}[\hat{H}, \hat{\rho}(t)] + \mathcal{L}\hat{\rho}(t), \quad (8)$$

where $\hat{\rho} = \sum_k p_k |k\rangle\langle k|$ denotes the reduced density matrix operator of the multilevel system, and $\mathcal{L}\hat{\rho}(t) = \sum_i \Gamma_i / 2 [2\hat{D}_i \hat{\rho}(t) \hat{D}_i^\dagger - \hat{D}_i^\dagger \hat{D}_i \hat{\rho}(t) - \hat{\rho}(t) \hat{D}_i^\dagger \hat{D}_i]$ with Γ_i denoting transition rate for the i -th dipole due to the background radiation pump, spontaneous, Coulombic and Auger decays, photodissociations, and collision processes. Here, the first term in the right side describes the coherent dynamics of the multilevel system coupled with the laser field, and the second term denotes the incoherent processes, such as spontaneous and Auger decays, transitions due to the black-body radiation field and collision processes. The contributions of the black-body radiation pump are only nontrivial in warm and hot matters, and collision processes can be neglected for the dilute atomic and molecular gases since it occurs in a fs timescale being much shorter than the average particle-collision time. Note that the broadening contributions of the incoherent-field-system interactions in Eq. (1) and plasma environments are included to the second term in Eq. (8), while the corresponding energy shifts are incorporated in the energy levels of the system in vacuum. We remark here that the thousand state master equation has unique features, which needs large-scale simulations for propagating in time a matrix of $\approx 10^6 \times 10^6$ and is not trivial to solve directly, such as stability of numerical linear algebra and parallel procedure demanding.

There are two possible ways to take photoionization processes into account in our simulations. While we treat the ionization as incoherent processes by adding photoionization cross section in the incoherent terms for

the low intensity X-ray laser, we consider ionization as coherent processes for multiphoton dominant processes, which features analogies to bound-state transitions of the system. For multiphoton dominant processes, the ionized state composing of the residual system and ionized electrons reads

$$|k\rangle = |j_{\text{core}}, \kappa; J, \epsilon_k, P\rangle, \quad (9)$$

where $j_{\text{core}}, \kappa, J, \epsilon_k, P$ denote the angular momentum of the residual system, relativistic angular momentum of free electrons, total angular momentum, total energy and parity of the system, respectively. In the physical systems, these states can be populated by multiphoton excitations. Considering the large amount of continuous states, selection rules should be used to solely include dominant states, such as degenerate initial, intermediate and final continuous states connected by multiphoton energies, and at the same time neglect states detuned from resonance excitations since the finite time duration of the X-ray laser implies a finite Fourier width for the bound-free or free-free transitions. These selections are a good approximation for hydrogen in the presence of strong laser beams, and therefore we anticipate that the dominant states for ionizations of a complex system should be similar.

Complementary to the multilevel master equation, in this work we employ a degenerate master equation approach to explore the physics of Eq. (1), which is computationally more affordable. Here, the Rabi frequency is $\sqrt{(2M_J + 1)(2M'_J + 1)}\Omega_i$ and the decay rate is defined as a total transition probability from one upper state $|J, M_J\rangle$ to all the degenerate lower states of the level $|J'\rangle$.

a. population distribution— Free states $|k\rangle$ form a complete basis set, and we can work in the set and obtain a number of algebraic equations for Eq. (8). Due to infinite number of matrix elements, however, truncation for a finite N -state basis is required. And then the full Eq. (1) is projected onto this subspace spanned by the N -basis states, and it is expected this projection gives the best possible description of dynamics of the system induced by an X-ray laser, such as a neon gas by including thousands of energy levels. After solving the multilevel master equation, we obtain population distributions for each level and coherence between different transition states as a function of time, by calculating $\rho_{kk'} = \langle k | \hat{\rho}(t) | k' \rangle$, and then comparison can be made with experimental data by utilizing ion charge-state spectra recorded by a time-of-flight analyzer [20], even though the recently typical free-electron lasers have limited temporal coherence and new techniques are needed to improve it.

Master equation approach can reduce to Einstein's rate equation approach, if the pump field is fully stochastic, such as a broadband isotropic light field. In this case, coherence embedded in the off-diagonal terms is neglected, and the time evolution of the system is characterized by the population changes for each energy level.

b. resonance fluorescence— The spectrum of resonance fluorescence in high-intensity x-ray pulses can also

be calculated via master equation approach [7, 53, 55–58]. The time-dependent spectrum of the fluorescent light, described by autocorrelation function of the electric field operator $\hat{E}(t)$, is given by [53, 59]

$$S(t, \omega) = \int_0^t \int_0^t e^{-i\omega(t_1-t_2)} \langle \hat{E}^-(t_1) \hat{E}^+(t_2) \rangle dt_1 dt_2, \quad (10)$$

where $\hat{E}^-(t)$ and $\hat{E}^+(t)$ denote negative and positive frequency parts of the electric field, respectively.

The change in time of the occupation number of photons can be related to the dipole moment operator, and it reads

$$\hat{E}^-(t) = C(\mathbf{r}) \hat{D}_i^\dagger(t), \quad (11)$$

where $C(\mathbf{r})$ is a proportionality factor at position \mathbf{r} and can be neglected in a homogeneous system. And then we obtain

$$S(t, \omega) = 2 \int_0^t dt_2 \int_0^{t-t_2} \text{Re} \left[e^{-i\omega\tau} \langle \hat{D}_i^\dagger(t_2 + \tau) \hat{D}_i(t_2) \rangle \right] d\tau \quad (12)$$

where we only include the contributions in the region $t_1 \geq t_2$ and introduce the time delay $\tau \equiv t_1 - t_2$.

Thus we need the knowledge of two-time expectation values of $\hat{A}_{ij}(t_1, t_2) = \hat{D}_j(t_1) \hat{D}_i(t_2)$ for the time-dependent fluorescent spectrum of the i -th dipole transition. Applying the quantum regression theorem [55, 56], we obtain the coupled equation for the i -th dipole transition,

$$\frac{d\hat{A}(t_1, t_2)}{dt_1} = -\frac{i}{\hbar} [\hat{H}(t_1), \hat{A}(t_1, t_2)] + \mathcal{L}\hat{A}(t_1, t_2), \quad (13)$$

where $t_1 \geq t_2$, and the initial condition can be obtained by the one-time evolution operator $A_{ij}(t_2, t_2) = \langle \hat{D}_j(t_2) \hat{D}_i(t_2) \rangle$ via Eq. (8).

C. Examples: dilute atomic gases

Before proceed to construct the master equation, we should first calculate the wavefunctions and energy levels of the system, and obtain the required data, including oscillator strength, dipole moment, Rabi frequency, spontaneous and Auger decay rates, and photoionization cross section. Actually, dilute atomic gases are widely used in the recently typical experiment [20]. From now on, we take dilute multielectron atomic gases as examples for discussing coherent dynamics of the rapidly decayed X-ray-matter systems. Without loss of generality, these discussions can be easily applied to other X-ray-matter systems, such as molecular gases and solid-state materials by calculating corresponding wavefunctions, energy levels and microscopic transition processes. Here, we can map the dilute atomic system into a single-atom problem each of which can be written as in Eq. (1). The computations of various atomic radiative processes involve the

bound and continuum states of different successive ionization stages in the single atom. For the bound states, a fully relativistic approach based on the Dirac equation is utilized, while for the continuum processes the distorted wave approximation is employed. The bound states of the atomic system are calculated in the configuration interaction approximation. The radial orbitals for the construction of basis states are derived from a modified self-consistent Dirac-Fock-Slater iteration on a fictitious mean configuration with fractional occupation numbers, representing the average electron cloud of the configurations included in the calculation. The detailed discussion can be found in Refs. [60–62].

c. Rabi frequency— In the dipole approximation, the Rabi frequency for the bound-state transition can be obtained from the degenerate emission oscillator strength of the electric dipole \hat{d}_i ,

$$\begin{aligned} g f_i &= \frac{2m_e}{3\hbar^2} \Delta E |\langle \hat{d}_i \rangle|^2 \\ &= 8.749 \times 10^{18} \times \Delta E |\langle \hat{d}_i \rangle|^2, \end{aligned} \quad (14)$$

and then it yields.

$$\begin{aligned} \Omega_i &= \frac{eE}{\hbar} \langle \hat{d}_i \rangle \\ &= 1.409 \times 10^9 \sqrt{I \times g f_i / \Delta E} \\ &\times (-1)^{J-M_j} \begin{pmatrix} J & 1 & J' \\ -M_J & q & M'_J \end{pmatrix}, \end{aligned} \quad (15)$$

where laser intensity I and transition energy ΔE are in units of W/cm² and eV, respectively. Here q denotes the polarization of the external laser, \hat{d}_i denotes the electric dipole moment for the $J \rightarrow J'$ transition between states $|J, M_J\rangle$ and $|J', M'_J\rangle$ with Zeeman structure, m_e denotes the mass of atom, E denotes the electric field, and e denotes the charge of electron.

For photoionization processes (bound-free transition), the cross section is given by the differential oscillator strength $\frac{df}{d\epsilon}$,

$$\begin{aligned} \sigma(\epsilon) &= 4\pi^2 \alpha a_0^2 \frac{df}{d\epsilon} \\ &= 8.067 \times 10^{-18} \times \frac{df}{d\epsilon}, \end{aligned} \quad (16)$$

where the energy ϵ is in unit of Ry, α denotes the fine-structure constant and a_0 denotes the Bohr radius. And then Rabi oscillation for bound-free processes can be written as:

$$\begin{aligned} \Omega &= \frac{eE}{\hbar} \langle \hat{d}_i \rangle \\ &= 0.135 \times 10^{18} \int g(\epsilon) \sqrt{I \times \sigma(\epsilon) / \Delta E} d\epsilon, \end{aligned} \quad (17)$$

where, I , σ and ΔE are in units of W/cm², cm² and eV, respectively, and $g(\epsilon)$ is the lineshape of the bound-free transition, such as broadening due to the finite period of time duration for the X-ray laser.

For free-free processes, the Rabi frequency of the $\kappa \rightarrow \kappa'$ transition with the residual ion in the state $|j_{\text{core}}\rangle$ can be given by:

$$\Omega = \frac{eE}{\hbar} \langle j_{\text{core}}, \kappa; J | \hat{d}_i | j_{\text{core}}, \kappa'; J' \rangle, \quad (18)$$

where κ and J denote the relativistic angular momentum of free electrons and the total angular momentum of the system, respectively.

d. Spontaneous decay— Even in the absence of an applied field, spontaneous emission cannot be ignored, since the excited state interacts with the vacuum fluctuations of the electromagnetic field. After integrating over all possible modes and summing over the two orthogonal polarizations possible for each wave vector, the spontaneous $|e\rangle \rightarrow |g\rangle$ transition rate is given by a perturbation treatment,

$$\begin{aligned} A_i &= \int g(\omega) |\Omega_i|^2 d\omega \\ &= \frac{e^2 \omega_0^3}{3\pi \epsilon_0 \hbar c^3} |\langle g | \hat{\mathbf{r}} | e \rangle|^2, \end{aligned} \quad (19)$$

where c is the speed of light, ϵ_0 denotes the permittivity, and ω_0 denotes the transition frequency. Here, one assumes the lineshape function $g(\omega)$ is sharply peaked around ω_0 , so that $\int_{\omega} g(\omega) |\langle g | \hat{\mathbf{r}} | e \rangle|^2 \omega^3 d^3\omega \approx |\langle g | \hat{\mathbf{r}} | e \rangle|^2 \omega_0^3 \int_{\omega} g(\omega) d^3\omega = 2\pi \omega_0^3 |\langle g | \hat{\mathbf{r}} | e \rangle|^2$.

e. Stimulated transition— If the $|g\rangle \rightarrow |e\rangle$ transition is driven by the external radiation field with photon polarization ϵ in the differential solid angle $d\Theta$, the transition rate in this solid angle Θ , based on Fermi's Golden rule, is written as:

$$\begin{aligned} dB_i &= \int \frac{e^2}{\hbar^2} |\langle e | \hat{\mathbf{r}} \cdot \epsilon | g \rangle|^2 \frac{\hbar\omega}{2\epsilon_0 V} \left(n_{\lambda}^{\epsilon} \frac{V}{(2\pi c)^3} \omega^2 \right) g(\omega) d\omega d\Theta \\ &= \int \frac{e^2 \omega^3}{2\hbar \epsilon_0 (2\pi c)^3} |\langle e | \hat{\mathbf{r}} \cdot \epsilon | g \rangle|^2 n_{\lambda}^{\epsilon} g(\omega) d\omega d\Theta \end{aligned} \quad (20)$$

with $|E|^2 = \frac{\hbar\omega}{2\epsilon_0 V} n_{\lambda}^{\epsilon} \frac{V}{(2\pi c)^3} \omega^2$.

As for black-body radiation field, energy density of its radiation varies slowly over the range of transition energies,

$$\int_{\omega} g(\omega) \rho(\omega) d\omega \approx \rho(\omega) \int_{\omega} g(\omega) d\omega = 2\pi \rho(\omega). \quad (21)$$

Considering the isotropic and unpolarized properties of the radiation field, the total transition rate can be obtained by integrating over all possible modes and summing over the two polarizations of the field:

$$B_i = \frac{e^2 \omega_0^3}{3\pi \epsilon_0 \hbar c^3} n_{\lambda} |\langle e | \hat{\mathbf{r}} | g \rangle|^2, \quad (22)$$

and correspondingly Einstein B coefficient

$$B_{Ei} = \frac{\pi e^2}{3\epsilon_0 \hbar^2} |\langle e | \hat{\mathbf{r}} | g \rangle|^2, \quad (23)$$

with energy density $\rho(\omega) = \hbar\omega^3 n_{\lambda} / \pi^2 c^3$. We remark here that the transition rate $B_i = A_i n(\omega)$, with $n(\omega)$ being the mean photon number of the incoherent field at frequency ω [6, 54], such as the black-body radiation field.

As for laser driven atomic system, one can use the relation between laser intensity I and photon number n_{λ}^{ϵ} with polarization ϵ and wavelength λ

$$I(\Theta)/c = n_{\lambda} \frac{\omega^2}{(2\pi c)^3} \hbar\omega, \quad (24)$$

and then obtains:

$$\begin{aligned} \frac{dB_i}{d\Theta} &= \int \frac{e^2}{2\hbar^2 \epsilon_0 c} |\langle e | \hat{\mathbf{r}} \cdot \epsilon | g \rangle|^2 I(\Theta) g(\omega) d\omega \\ &= \int \frac{e^2}{6\hbar^2 \epsilon_0 c} |\langle e | \hat{\mathbf{r}} | g \rangle|^2 I(\Theta) g(\omega) d\omega, \end{aligned} \quad (25)$$

where one averages over all the polarization directions of the dipole moment. Normally, the laser injects from one certain direction with central frequency ν ($I(\Theta)d\Theta = I(\nu)\delta(\Theta)d\Theta$), and in this case the total transition rate can be written as:

$$B_{ge} = \frac{\pi e^2}{3\hbar^2 \epsilon_0 c} |\langle e | \hat{\mathbf{r}} | g \rangle|^2 \int I(\nu) g(\nu) d\nu \quad (26)$$

where $g(\nu)$ is the line shape of the $|g\rangle \rightarrow |e\rangle$ transition.

If one defines absorption (emission) cross section as:

$$\begin{aligned} \sigma_i(\nu) &= B_i h\nu / I(\nu) \\ &= \frac{2\pi^2 e^2 \nu}{3\epsilon_0 \hbar c} |\langle e | \hat{\mathbf{r}} | g \rangle|^2 g(\nu), \end{aligned} \quad (27)$$

one obtains

$$\begin{aligned} B_i &= \int_{\nu} \sigma_i(\nu) \frac{I(\nu)}{h\nu} d\nu \\ &= \int_{\nu} \frac{I(\nu)}{h\nu} \frac{\pi e^2}{2\epsilon_0 m_e c} f_i g(\nu) d\nu \\ &= 109.761 \times 10^{-18} \times \\ &\quad \int_{\omega} \frac{I(\omega) f_i}{\hbar\omega} \frac{\hbar A_i / 2\pi}{(\hbar\omega - \hbar\omega_i)^2 + (\hbar A_i / 2)^2} d\omega, \end{aligned} \quad (28)$$

where the full-width-half-maximum $\Delta\nu = A_i / 2\pi$, and laser intensity I and photon energy $\hbar\omega$ are in units of W/cm^2 and eV , respectively.

f. Autoionization— Complex atoms, irradiated by X-ray laser, can form hole atoms and then relax in a fs timescale via Auger decay processes, i.e. spontaneously emitting one of the electrons in along with refilling the hole by outer-shell electrons. The corresponding autoionization rate is expressed as

$$A_i^a = 2 \sum_{\kappa} \left| \left\langle j_{\text{core}}, \kappa; J, M_J \left| \sum_{m < n} \frac{1}{\mathbf{r}_{mn}} \left| J', M_J' \right. \right. \right\rangle \right|^2, \quad (29)$$

where κ is the relativistic angular quantum number of the ionized electron, and \mathbf{r}_{mn} denotes the relative displacement of between electrons m and n . Here, J and

M_J denote total angular momentum and magnetic quantum number of the system consisting of the residual ion and ionized electrons, respectively.

For some cases, double Auger processes are nontrivial and should be included in the simulations, and the code for the atomic data of direct two-electron processes has been developed recently [63]. In this work, we do not include the contributions from the direct double Auger processes, yet its implementation in the master equation is straightforward.

III. RESULTS

In this section, we discuss coherent dynamics of the rapidly decayed X-ray-matter systems. As examples, we investigate ultrafast dynamics of inner-shell electrons of complex atoms irradiated by an X-ray laser via a thousand state master equation approach. The influence of coherence on dynamical mechanics will be investigated through comparisons between atomic systems induced by X-ray pulses with different temporal coherence. For ionizations, multiphoton ejections of electrons from an atom subjected to a strong laser field will be investigated in the framework of master equation approach, where the reliability of our numerical results will be verified against the time-dependent Schrödinger equation. For inner-shell dynamical processes, Auger and spontaneous decay processes typically occur in a fs timescale and compete with other mechanics, such as coherent Rabi oscillations, where we will discuss possible experimental implementations such as signatures for coherent evolution of inner-shell electrons. Finally, we will discuss a *real* coherent dynamics of complex atoms induced by an X-ray laser, based on master equation approach by including thousands of atomic levels.

A. Coherent dynamics between bound states

In this section, we investigate coherent dynamics between bound states of an atomic system coupled by a X-ray laser, and pay special attention to the influence of coherence on dynamical evolution by comparing with Einstein's rate equation, which is a reduction of master equation approach and a method for the system illuminated by a broadband isotropic light field (incoherent light).

First we study the time evolution of a two-level H-like neon with atomic data being obtained via solving Dirac equation [60–62]. Due to the pump of the laser beam and coupling with the external environment, it is expected that the system exhibits a Rabi-oscillating feature, and then decays to a steady state after a longer time. As shown in the upper panel of Fig. 2, we observe Rabi oscillations between $|J = 0.5, M_J = 0.5\rangle$ ($1s$) and $|J = 1.5, M_J = 1.5\rangle$ ($2p$), and, after a few fs, steady states are achieved with the excited-state population be-

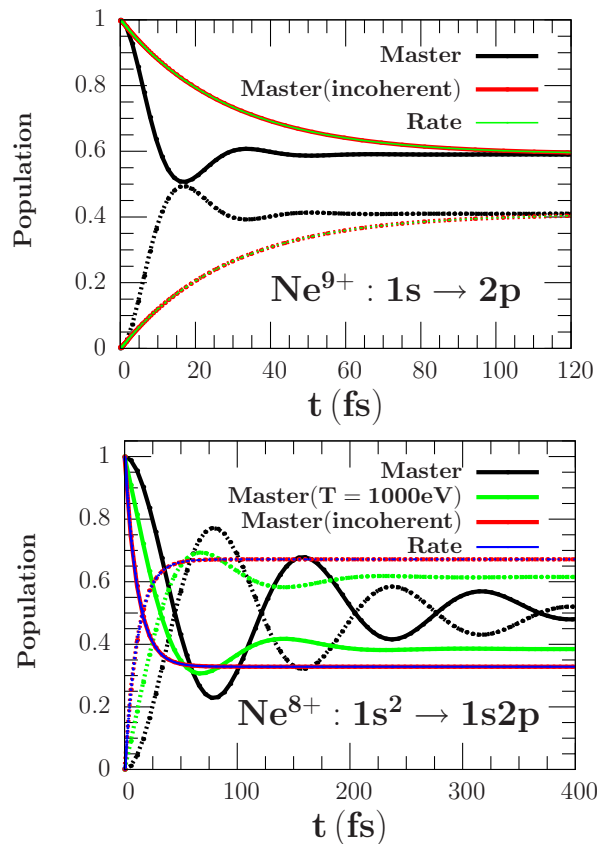


FIG. 2: Comparison with rate equation. **Upper:** State populations of a two-level H-like neon (between $|J = 0.5, M_J = 0.5\rangle$ of $1s$ and $|J = 1.5, M_J = 1.5\rangle$ of $2p$) as a function of time. **Lower:** Degenerate state populations for the transition $|J = 0\rangle \rightarrow |J = 1\rangle$ ($1s^2$ - $1s2p$) of He-like neon. Here, the solid and dashed lines denote populations of the ground and excited states, respectively, coupled by a laser with an intensity $I_0 = 10^{12}$ W/cm². For the incoherent pump, master equation yields identical results with those from the rate equation.

ing $\sqrt{\Omega^2/(\Gamma^2 + 2\Omega^2)}$. We observe that the stable states of master equation at a longer time are identical with rate equation approach, whose conclusion is also consistent with analytical results.

Then we investigate a multilevel atom interacting with an isotropic and unpolarized radiation beam, as relevant to Einstein's rate equation. We focus on the dipole transition $|J = 0\rangle \rightarrow |J = 1\rangle$ ($1s^2$ - $1s2p$) of He-like neon, where there are four states in the reduced Hilbert space and the upper three levels with angular momentum $|J = 1\rangle$ are triply degenerate due to magnetic splitting. We assume the ground state $|J = 0\rangle$ are populated at $t = 0$, and then switch on the pump laser. We observe a decayed Rabi-flopping structure in the master equation, due to the coupling with the pump laser and the external environment, while in the rate equation there is a monotonous decay for the ground state, as shown in the lower panel of Fig. 2. We also observe that both methods cannot yield identical stable states at a longer time. It

indicates that, for a multilevel atom coupled by a laser field, coherence influences both short-time structures and long-time stable states, and Einstein's rate equation approach cannot give reasonable results since coherence is totally neglected in this method. The coherence effects can also be clearly seen in Sec. III D.

Another issue needed to be addressed is the influence of different temporal coherence of the pump field on the dynamics of complex atoms. To simplify our discussion, an incoherent thermal radiation field is taken into account as incoherent pump sources, in addition to a coherent X-ray laser. It is expected that the interplay between coherent and incoherent pump influences dynamical properties of the atomic system. For example, the incoherent thermal radiation field can be introduced via $R_{J,J'} = \Gamma_{J,J'} \bar{n} = \Gamma_{J,J'} \{\exp[\hbar(\omega_{J'} - \omega_J)/kT] - 1\}$, where T is the temperature of the incoherent thermal radiation field, \bar{n} is average number of thermal photons per mode at each transition frequency, and $\Gamma_{J,J'}$ denotes the spontaneous decay induced by vacuum (the energy shift due to coupling with vacuum is included in \hat{H}_a). In the lower panel of Fig. 2, we show results for an atomic system coupled with a coherent field and a thermal radiation field of $T = 1000$ eV, and find that the stable states shift closer to those obtained from rate equation. For a fully incoherent pump in the framework of master equation approach, we find that the time evolution of the multilevel system coincides with Einstein's rate equation approach.

B. Coherent dynamics for photoionizations

g. Comparison with time-dependent Schrödinger equation for hydrogen— Ionization is a basic process of atoms subjected to an external electromagnetic field. For weak laser fields, perturbation theory can be utilized to capture these processes. For example, one considers a system prepared in an initial state $|i\rangle$ and perturbed by a periodic harmonic potential $V(t) = Ve^{i\omega t}$ which is abruptly switched on at time $t = 0$. Based on time-dependent perturbation theory, the first two basis coefficient c_n can be expanded as: $c_n^{(1)} = \frac{2\pi}{\hbar^2} |\langle f|V|i\rangle|^2 \delta(\omega_{fi} - \omega)$ corresponding to Fermi's golden rule, and $c_n^{(2)} = \frac{2\pi}{\hbar^4} \sum_m |\frac{\langle f|V|m\rangle\langle m|V|i\rangle}{\omega_m - \omega_i - \omega}|^2 \delta(\omega_{fi} - 2\omega)$ associating with two-photon processes, where $|i\rangle$, $|m\rangle$ and $|f\rangle$ denote the initial, intermediate and final states, respectively. In the study of atomic dynamics, one can simply include photon ionizations as decay coefficients up to the corresponding order, just as used in rate equation approach, where the coherence in ionization processes is totally neglected. For intense laser fields, however, multiphoton ejections of one electron typically occur, and manifest as dominant mechanics [20, 64–66]. In this case, the perturbation theory lacks the possibility for understanding multiphoton absorptions, and a nonperturbative treatment is inevitable to address this issue. Here, we describe coherent multiphoton ionizations in the framework of

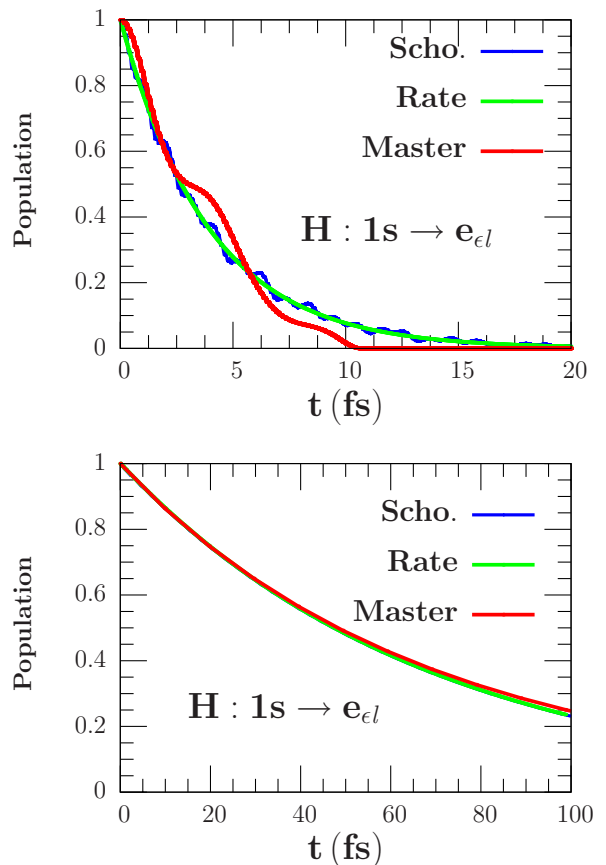


FIG. 3: Comparison with time-dependent Schrödinger equation. Ground-state populations of hydrogen as a function of time for a laser intensity $I_0 = 10^{14}$ W/cm² with photon energies of 14 eV (upper) and 30 eV (lower), respectively, obtained via rate equation, master equation and time-dependent Schrödinger equation.

the atomic master equation approach, and the validity of approach will be verified via comparisons with time-dependent Schrödinger equation where both the discrete and continuous states are treated in the same level.

In the calculations here, remarkable agreements between master equation and time dependent Schrödinger equation have been obtained for real dynamics of hydrogen in the intermediate-wavelength regime. In Fig. 3, for example, we show the ground-state evolution of hydrogen induced by a strong laser field with an intensity of 10^{14} W/cm², and photon energies of 14 eV and 30 eV, respectively, and find that the master equation approach can capture photoionization processes of hydrogen in the intermediate-wavelength regime. Surprisingly, rate equation offers another possibility to address this issue at these parameter regimes, even though the detailed structures are different, which indicates that the leading order process dominates ionizations here, irrespective of coherence or incoherence. We anticipate that photoionization mechanism for complex atoms in the X-

ray-wavelength regime should also be captured by master equation approach.

h. Coherence in photoionizations of neon— In this section, we discuss ionizations of complex atoms in the short-wavelength regime. In this regime, time-dependent Schrödinger equation encounters difficulties for dealing with electron-electron correlations and irreversible processes, such as Auger and spontaneous decay processes, while rate equation approach, mainly based on photoionization cross sections, fully discards coherence effects in the dynamical processes. The underlying physics for ionizations of both outer- and inner-shell electrons of complex atoms and its relevant dynamics induced by intense X-ray lasers are still unclear. Here, we will address this issue related to ionizations of complex atoms driven by a strong X-ray laser, based on master equation approach whose validity has been verified against ionizations of hydrogen as a benchmark.

In contrast to simple species such as hydrogen, the responses of neon subjected to X-ray laser beams for valence and inner-shell electrons are different, since Rabi frequency for valence electrons is comparable to free-free excitations, while the frequency for inner-shell electrons is much larger than free-free processes. We find that inner-shell electrons are ionized much faster than outer-shell electrons, as shown in Fig. 4 where ionizations of valence (upper panel) and inner-shell electrons (lower panel) of neon are triggered by an X-ray laser beam with a typical experimental intensity of 10^{18} W/cm² and photon energy of 875 eV. Comparisons between rate equation and master equation are made and remarkable agreements are obtained, even though tiny differences can be found in the detailed structures, due to coherent oscillations for ionizations in master equation approach. As far as we know, this is the first direct proof for coherent ionizations of both outer- and inner-shell electrons of neon in the short-wavelength regime, where sequential single-photon processes dominate the absorptions for the recently typical experimental conditions. This conclusion is consistent with the recent X-ray experiments, where one did not observe clear signatures of multiphoton single-electron ionizations. Hence it is not surprising that comparisons between theories and experiments suggest the dominant absorptions of electrons are sequential single-photon processes in Young’s experiment [20].

C. Coherent dynamics in Auger decay processes

In addition to ionizations of inner-shell electrons, Auger decay is another dominant process for complex atoms, which carries valuable information about inner-shell electronic structures and dynamical properties of atoms, molecules, and solids. Specifically, inner-shell electrons can be excited or ionized by the X-ray laser beam and a hole atom is formed. The atom is normally unstable and relaxes through Auger and spontaneous decay processes, which typically occurs in the fs timescale

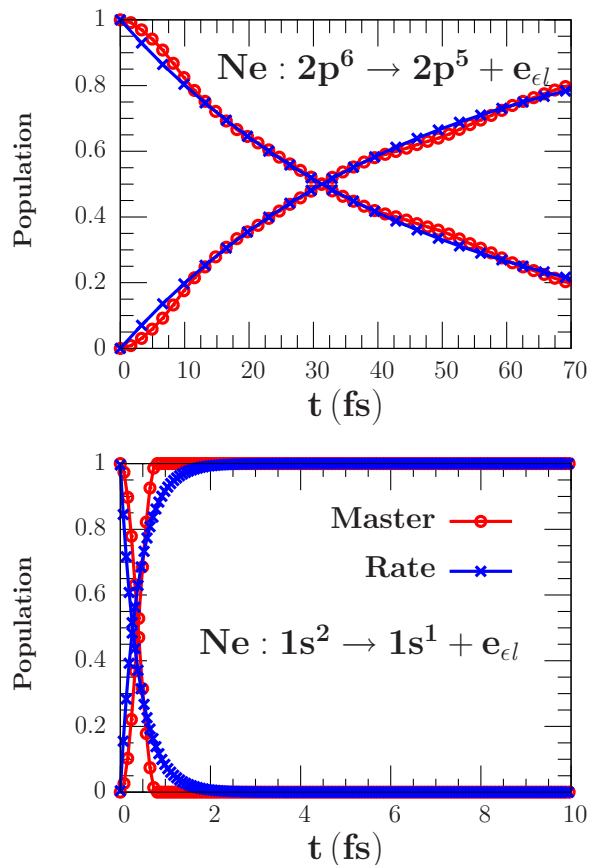


FIG. 4: Ionization of valence electrons (upper) and inner-shell electrons (lower) of a neon gas induced by an X-ray laser for a laser intensity of 10^{18} W/cm² with photon energy of 875 eV, obtained by master equation (red) and Einstein’s rate equation approach (blue), respectively. We find that single-photon processes for both outer- and inner-shell electrons dominate ionizations for the recently typical experiments with a laser intensity of $\approx 10^{18}$ W/cm².

and can smear out coherence-induced signals embedded in Rabi oscillations. In this section, we will investigate the competitions between Rabi oscillations, photoionizations, Auger and spontaneous decays, since the magnitudes of these processes are typically of the same order. These processes, however, are normally beyond the time revolution of the X-ray experiments. Fortunately, resonant fluorescence provides another available tool for studying these competitions and underlying coherence effects.

In our simulations, we study dynamical evolution of ground-state neon subjected to X-ray pulses with different temporal coherence and resonant photon energy relative to $1s^2 2s^2 2p^6 \rightarrow 1s^1 2s^2 2p^6 3p^1$ transition. After shining the X-ray laser on neon, inner-shell electrons are coherently excited and coupled between $1s$ and $3p$ orbitals. On the other hand, the hole state $1s^1 2s^2 2p^6 3p^1$ is unstable and decays in a fs timescale, mainly due to Auger decay processes by refilling the inner $1s$ orbital

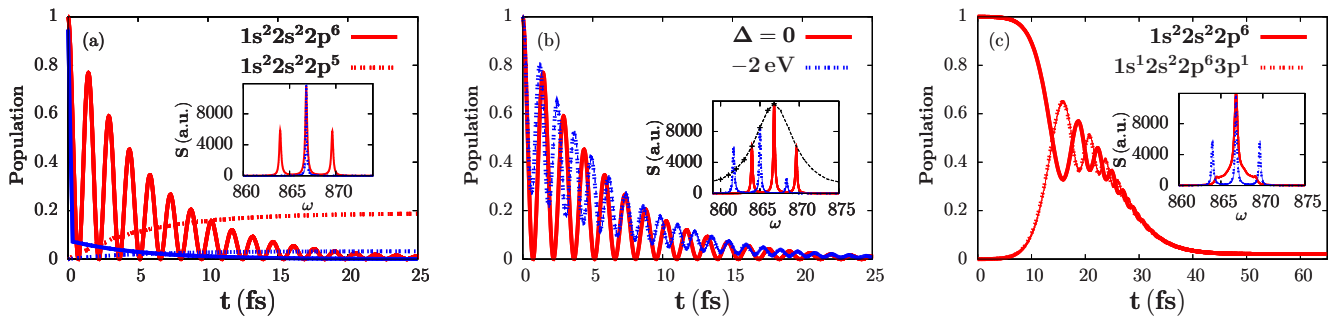


FIG. 5: Competition between Rabi oscillations, Auger and spontaneous decays, and photoionizations of a neon gas induced by an X-ray laser beam with a peak intensity of 10^{18} W/cm 2 . (a) Populations of degenerate states $1s^2 2s^2 2p^6$ (solid) and $1s^2 2s^2 2p^5$ (dashed) coupled by a flat-topped X-ray laser beam with a resonant photon energy for the $1s \rightarrow 3p$ transition, obtained via master equation (red) and rate equation approach (blue), with the inset for the fluorescence spectrum of the $1s^2 2s^2 2p^6 \rightarrow 1s^1 2s^2 2p^6 3p^1$ transition. (b) Ground-state populations of Ne for a resonant $1s \rightarrow 3p$ (red) and a red detuned pump $\Delta = -2$ eV (blue), where the inset shows the fluorescence spectrum of the $1s^2 2s^2 2p^6 \rightarrow 1s^1 2s^2 2p^6 3p^1$ transition with the black dashed line being the power-broadening guideline for the central peak. (c) Neon gases driven by a Gaussian X-ray pulse of a FWHM duration 15 fs, with the inset for fluorescence spectrum of $1s^2 2s^2 2p^6 \rightarrow 1s^1 2s^2 2p^6 3p^1$ transition (red) and those driven by a flat-topped pulse with the identical fluence (blue).

by the outer-shell electrons, or spontaneous decays of $2p$ and $3p$ electrons. The hole state can also be further ionized with double-core forming or via sequential valence electrons. To investigate the interplay between these different processes driven by X-ray pulses, we include all the dominant microscopic processes. We observe a decayed Rabi-flopping structure between $1s$ and $3p$ states coupled by an X-ray laser, based on master equation approach, while it is absent in rate equation method with a monotonous population changing. It indicates that the atomic coherence is distinctly embodied in Rabi oscillations driven by the X-ray laser, in spite of extremely fast Auger decays in the fs timescale. At present, however, one lacks reliable tools for observing these fast Rabi oscillations by real-time X-ray images experimentally. Fortunately, the coherent dynamical information for inner-shell processes can be extracted from fluorescence spectra, based on master equation approach.

As shown in the inset of Fig. 5(a), we observe a triple-peak structure for the resonance fluorescence of the $1s^2 2s^2 2p^6 \rightarrow 1s^1 2s^2 2p^6 3p^1$ transition, while only one central peak occurs for incoherent light pump. Considering the remarkable shift (≈ 2 eV) of the satellite line from the central peak for a laser intensity of 10^{18} W/cm 2 , the triple-peak spectra provide a valuable tool for studying Rabi floppings and are expected to be detected via recording photons from spontaneous radiative decays [25]. The next issue is related to the stability of the triple-peak structure against different experimental conditions, such as laser detuning and pulse shapes. We find that the triple-peak structure is stable. Specifically, we observe that the side peaks demonstrate asymmetric along with a red shift of the central peak for a red-detuned pump, as shown in Fig. 5(b), whereas a Gaussian X-ray pulse with a FWHM duration of 15 fs yields a broadened triple-peak structure compared to the flat-topped pulse, as shown in Fig. 5(c). Note that we

also observe a ≈ 5 eV broadening due to the extreme strong X-ray laser with an intensity of 10^{18} W/cm 2 , as shown in the guideline in the inset of Fig. 5(b), which is normally referred to as power broadening as will be discussed in Sec. III D. We expect that our discussions provide valuable insight for investigating inner-shell coherent dynamics in the upcoming experiments.

D. Real coherent dynamics of a neon gas irradiated by an X-ray laser

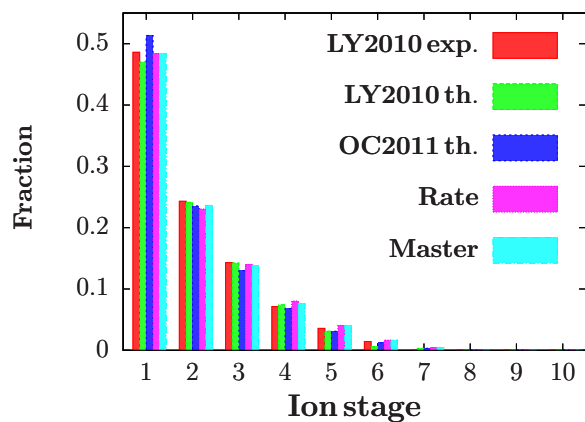


FIG. 6: Neon charge-state yields by a far off-resonant beam with photon energy of 800 eV. Good agreements between different theories [20, 30] and experiments [20] indicate that coherence, induced by a far off-resonant laser beam, plays a tiny role in the time evolution for the present experimental conditions.

In former sections, coherence effects have been investigated through ultrafast dynamics of model systems coupled by X-ray pulses with different temporal coherence.

In this section, we will investigate coherence effects beyond model systems, and take neon as examples for *real* dynamics of complex atoms induced by an X-ray laser, based on master equation approach by including thousands of atomic levels. The X-ray laser can sequentially excite inner-shell electrons and creates a nonequilibrium state decayed through a vast number of channels. To simplify our simulations, we add the atomic orbitals gradually, and mainly focus on dynamics of the lowest-lying orbitals of neon, such as $1s$, $2s$, $2p$, $3n$ and $4n$, and inner-shell excited states $1s2n^2$, $1s2n3p$ and $1s2n4p$ as well, which normally includes atomic levels up to an order of 10^3 and spans the Hilbert subspace as basis states for *real* dynamics of neon. Our selections are supported by the recent R-matrix calculations for inner-shell electrons [67]. After obtaining atomic data, we study the interplay between coherence-induced effects and dissipations in X-ray-atom systems, based on large scale simulations. We will verify to which extent coherence demonstrates a dominant role in the ultrafast decayed nonequilibrium system.

i. Off-resonant dynamics of neon in Young's experiment— First we review the details of the X-ray free-electron-laser experiment for neon in Ref. [20]. In this experiment, X-ray pulses with photon energies of 800, 1050 and 2000 eV are injected into a neon gas in the atomic chamber, and they observe rapid photoabsorptions of atomic gases in the fs timescale. As pointed out in the experiment, effects due to particle collisions and photon scattering can be neglected, since the neon gas is dilute and induced by pulses with photon energies below 8 keV. Therefore, photoabsorptions are the dominant processes of neon triggered by the X-ray beam in the ultra-intense, short-wavelength regime. Here, we take photon energy of 800 eV as examples for investigating the influence of coherence on the sequential multiphoton ionizations of the neon gas, where the photon energy is far below resonant $1s \rightarrow 3p$ excitations and it is referred to as off-resonant dynamics of neon. Remarkable agreements are obtained between different theories [20, 30] and experiments [20], as shown in Fig. 6, which indicates that coherence plays a tiny role in the time evolution of neon induced by a far off-resonant X-ray pulse in the present experiments. For comparisons, here we use both Gaussian and flat-topped pulses to simulate the experimentally accessible dynamics of inner-shell electrons of neon, and find that the charge-state distributions is insensitive to the pulse shapes.

j. Near-resonant dynamics of inner-shell electrons of neon— In this paragraph, we study the time evolution of neon subjected to a strong X-ray laser field with near-resonant photon energies, based on large scale simulations by including energy levels in an order of 10^3 . In Fig. 7, we demonstrate charge state populations as a function of time for a laser intensity $I_0 = 2.5 \times 10^{17} \text{ W/cm}^2$, which is a typical free-electron-laser intensity in the recent experiments, obtained via master equation [solid line in Fig. 7(a),(b),(c)] and rate

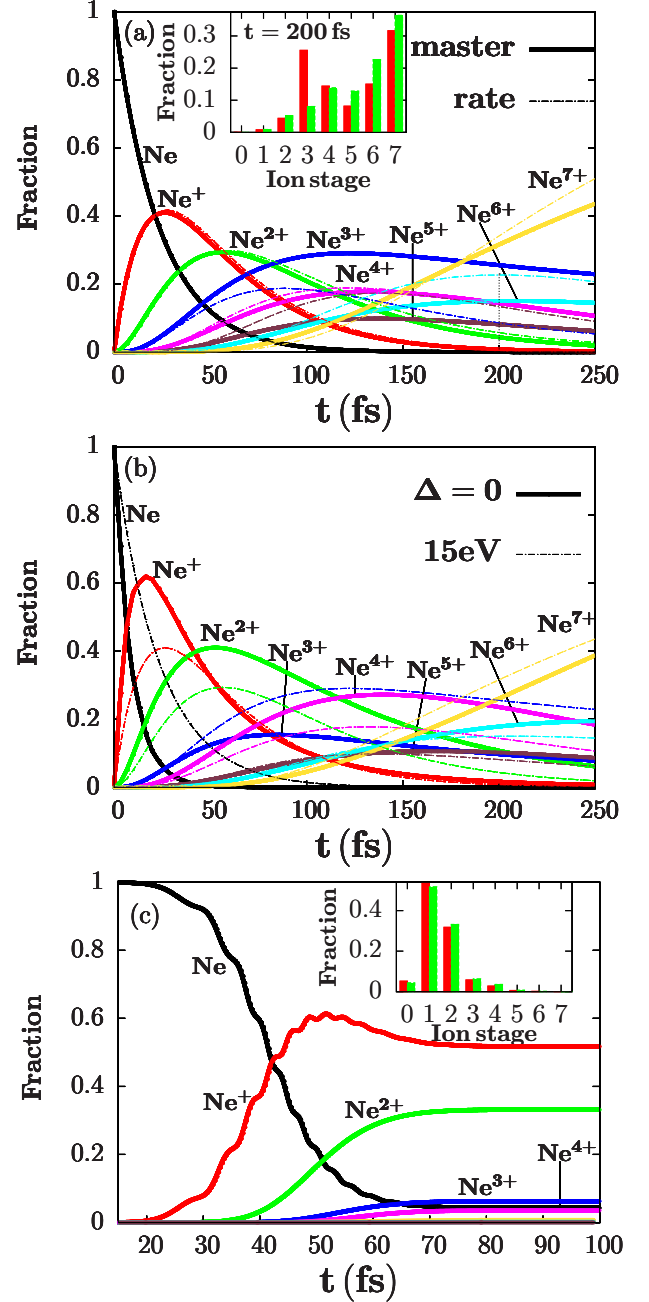


FIG. 7: Coherence-induced suppression on time evolution: charge-state populations of neon induced by the X-ray laser with an intensity of $2.5 \times 10^{17} \text{ W/cm}^2$ for different photon energies: near-resonant excitation with a red detuning of 15 eV (a) and resonant photoexcitation [(b),(c)] for $1s^2 2s^2 2p^6 \rightarrow 1s^1 2s^2 2p^5 3p^1$ transition, and for different pulse shapes: flat-topped [(a),(b)] and Gaussian pulses of a FWHM duration 25 fs (c). Discrepancies between master equation and rate equation are the results of coherence-induced Rabi oscillations and power-broadening effects. **Inset:** Fraction yields for different charge stages of neon obtained by master equation (red) and rate equation (green) for a pulse duration of 200 fs (a), and induced by a Gaussian pulse (red) of a FWHM duration 25 fs and a flat-topped pulse (green) with the same fluence (c).

equation approach [dashed line in Fig. 7(a)]. The photon energies are chosen near resonant frequency relative to the $1s^22s^22p^6 \rightarrow 1s^12s^2p^63p^1$ transition, such as a red shift of 15 eV [Fig. 7(a),(b)] and the resonant case [Fig. 7(b),(c)], which are both in the photon-energy range of LCLS (800-2000 eV). We find that coherence can suppress the multiphoton ionizations of neon induced by the ultra-intense X-ray pulse. As shown in the inset of Fig. 7(a), for example, the charge state population of Ne^{3+} after a 200 fs evolution, is twice bigger than that obtained by rate equation approach for incoherent pumping with an intensity of $2.5 \times 10^{17} \text{ W/cm}^2$. The physical origin of the discrepancy in the time evolution is the results of two effects, which are neglected in the Einstein's rate equation. The first one is the coherence in the inner-shell resonant absorption processes, i.e $1s \rightarrow 3p$ excitations for Ne and $1s \rightarrow 2p$ for Ne^{3+} , Ne^{4+} and Ne^{5+} . In contrast to monotonous changes in rate equation approach, real physical processes between different energy levels demonstrate a Rabi-flopping structure, due to the light-atom coupling for the $1s \rightarrow 2p$ and $1s \rightarrow 3p$ transitions. The second one is the power broadening effects, due to the extremely strong X-ray laser field, which can be up to an order of a few eV at a laser intensity of $2.5 \times 10^{17} \text{ W/cm}^2$, based on a two-level estimation $\sqrt{\gamma^2 + 2\Omega^2}$ with γ and Ω being spontaneous decay rate and Rabi frequency, respectively. This point can also be verified via fluorescence spectra, as shown in the inset of Fig. 5(b). Interestingly, we find that the red-shift case (relative to $1s \rightarrow 3p$ transition) ionizes more electrons after 150 fs evolution, since the $1s \rightarrow 2p$ excitations of inner-shell electrons come into play for charge states Ne^{3+} , Ne^{4+} and Ne^{5+} , whereas the resonant case ionizes electrons fast in the early stage after subjected to the X-ray laser field, since the resonant $1s \rightarrow 3p$ excitations dominate photon absorptions of Ne in the first 50 fs, as shown in Fig. 7(b). The influence of temporal pulse shape on the charge-state distributions is also discussed in Fig. 7(c), where comparison has been made between flat-topped (green) and Gaussian pulses (red) in the inset. We remark here that the temporal pulse shape has limited impact on the charge state distributions, whose conclusion is consistent with those for incoherent pulses [20].

Next, we address the issue related to power broadening effects in more details. Actually, the broadening effect, resulting in the line shape of a dipole transition in an atom, is a basic feature for describing electron motions and interactions with external fields. The underlying mechanisms of broadening effects are diverse, including natural broadening due to spontaneous decays of excited states, Doppler broadening due to thermal motions of atoms, collisional broadening due to collisions with other atoms or ions, and Stark broadening due to energy shifts induced by an external field. Here, we find that the dominant broadening effect for the dilute neon gas in the LCLS experiment is the power broadening (≈ 1 eV) due to the extremely strong external laser, which is up to 10 times bigger than those from Auger and spon-

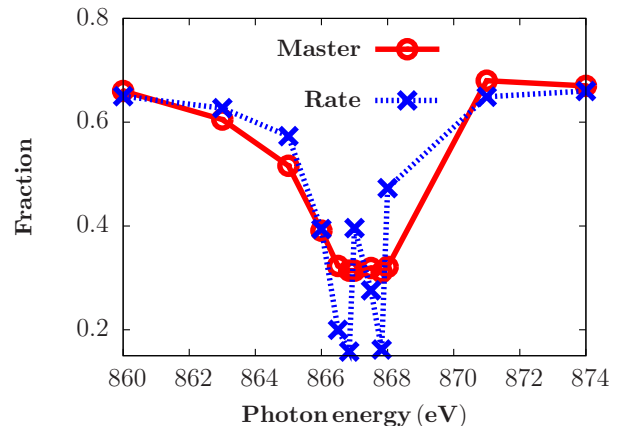


FIG. 8: Power broadening effects: Ne fraction in a neon gas subjected to a Gaussian X-ray pulse with an intensity of $2.5 \times 10^{17} \text{ W/cm}^2$ and a FWHM duration of 10 fs, for different photon energies, obtained by master equation (red solid) and rate equation approach (blue dashed).

taneous decay processes (≈ 0.1 eV). Normally the rate equation approach does not include the power broadening effects in the present calculations, while in the master equation approach they are included automatically. In Fig. 8, we show the Ne fractions subjected to a Gaussian X-ray laser with an intensity of $2.5 \times 10^{17} \text{ W/cm}^2$ and a FWHM duration of 10 fs, where two local minima, obtained from rate equation (blue dashed), correspond to resonant excitations for $1s^22s^22p^6 \rightarrow 1s^12s^22p^63p^1$ and $1s^22s^22p^6 \rightarrow 1s^12s^22p^64p^1$ transitions, respectively. However, the oscillating structures for resonant excitations at different photon energies are smoothen in the results obtained from master equation approach (red circle), due to power broadening effects. Note here that the oscillating structures can occur at other photon energies associated with $1s \rightarrow np$ ($n \geq 5$) transitions, but are beyond the spectrum resolution in the present experiments and an improved sharp-band X-ray laser is needed in the future.

IV. SUMMARY AND OUTLOOK

In conclusion, we establish a general method for describing coherent dynamics of X-ray-matter systems in the framework of master equation approach. We take dilute atomic gases as examples for discussing *real* coherent dynamics of the rapidly decayed X-ray-matter system, based on a thousand state atomic master equation approach, by including coherent pump and incoherent relaxations due to spontaneous and Auger decays. We find that coherence can suppress the sequential single-photon ionizations of a neon gas in the ultra-intense X-ray field, compared to the rate equation approach, and the physical reason can attribute to the coherence-induced Rabi oscillations and power broadening effects, which are both

neglected in the Einstein's rate equation. We also find that single-photon ionizations for both outer- and inner-shell electrons dominate the absorptions of a neon gas for the recently typical experiments with a laser intensity of $\approx 10^{18}$ W/cm², irrespective of coherence. A typical feature of coherent evolution of inner-shell electrons is Rabi oscillations with a frequency in the order of 10^{15} Hz, which is beyond the current experimental resolutions in the time domain. Instead, we discuss resonance fluorescence spectra for possible experimental implementations for coherent dynamics of inner-shell electrons.

With the quick development of free-electron lasers, temporal coherence of the X-ray laser is improved experimentally, which provides the possibility for studying time-resolved coherent phenomena in atoms, molecules and solid-state materials [68]. There are still a number of open issues referred to coherent dynamics of complex systems irradiated by an intense X-ray laser. For the methods described here, we are able to discuss hollow-atom signatures and its corresponding coherent dynamics, where the competition between the double- and single-hole generations in coherent evolution is still un-

clear. Moreover, we can also investigate multiphoton processes of atoms and molecules in gases and solid-dense matters, such as two-photon KK-shell transitions, where the issues are related to non-sequential double ionizations and electron-electron correlations. Finally, in a dense hot plasma environment generated by dense gases or solid-state materials induced by an X-ray laser, the environment is much more complicated, both radiative and particle-collision processes should be taken into account for understanding the phenomena of the system.

Acknowledgments

We acknowledge useful discussions with Z.-X. Zhao and H.-Y. Sun. This work is supported by the National Basic Research Program of China (973 Program) under Grant No. 2013CB922203, the National Natural Science Foundation of China under Grant Nos. 11274383, 11304386, 11104350 and 11204376.

-
- [1] L. Diósi and L. Ferialdi, *Phys. Rev. Lett.* **113**, 200403 (2014).
- [2] F. Kadi, T. Winzer, E. Malic, A. Knorr, F. Götfert, M. Mittendorff, S. Winnerl, and M. Helm, *Phys. Rev. Lett.* **113**, 035502 (2014).
- [3] T. Ambjörnsson, S. K. Banik, O. Krichevsky and R. Metzler, *Phys. Rev. Lett.* **97**, 128105 (2006).
- [4] Y.-J. Wei, Y. He, Y.-M. He, C.-Y. Lu, J.-W. Pan, C. Schneider, M. Kamp, S. Höfling, D. P. S. McCutcheon and A. Nazir, *Phys. Rev. Lett.* **113**, 097401, (2014).
- [5] A. C. Pflanzner, O. Romero-Isart and J. I. Cirac, *Phys. Rev. A* **86**, 013802 (2012).
- [6] A. Imamoglu, J. E. Field and S. E. Harris, *Phys. Rev. Lett.* **64**, 1154 (1991).
- [7] S. M. Cavaletto, C. Buth, Z. Harman, E. P. Kanter, S. H. Southworth, L. Young and C. H. Keitel, *Phys. Rev. A* **86**, 033402 (2012).
- [8] J. Seres, E. Seres A. J. Verhoef, G. Tempea, C. Strelti, P. Wobrauschek, V. Yakovlev, A. Scrinzi, C. Spielmann and F. Krausz, *Nat. (London)* **433**, 596 (2005).
- [9] T. H. Maiman, *Nat. (London)* **187**, 493 (1960).
- [10] U. Fano, *Phys. Rev.* **124**, 1866 (1961).
- [11] J. F. Annett, *Superconductivity, Superfluid and Condensates*, (Oxford University Press 2004).
- [12] E. A. Cornell and C. E. Wieman, *Rev. Mod. Phys.* **74**, 875 (2002); W. Ketterle, *Rev. Mod. Phys.* **74**, 1131 (2002).
- [13] S. E. Harris, *Phys. Today* **50**, 36 (1997); A. Imamoglu and S. E. Harris, *Opt. Lett.* **14**, 1344 (1989).
- [14] L. Plaja, R. Torres, A. Zair, *Attosecond Physics: Attosecond Measurements and Control of Physical Systems*, (Springer London Press 2013).
- [15] K.-J. Boller, A. Imamoglu, and S.E. Harris., *Phys. Rev. Lett.* **66**, 2593 (1991).
- [16] M. Greiner, O. Mandel, T. Esslinger, T. W. Hänsch and I. Bloch, *Nat. (London)* **415**, 39 (2002).
- [17] P. Emma *et al.*, *Nat. Photon.* **4**, 641 (2010).
- [18] F. Lehmkuhler *et al.* *Sci. Rep.* **4**, 5234 (2014).
- [19] B. Nagler *et al.*, *Nat. Phys.* **5**, 693 (2009).
- [20] L. Young, E. P. Kanter, B. Krässig, Y. Li, A. M. March, S. T. Pratt, R. Santra, S. H. Southworth, N. Rohringer, L. F. DiMauro, G. Doumy, C. A. Roedig, N. Berrah, L. Fang, M. Hoener, P. H. Bucksbaum, J. P. Cryan, S. Ghimire, J. M. Glowonia, D. A. Reis, J. D. Bozek, C. Bostedt and M. Messerschmidt, *Nat. (London)* **466**, 56 (2010).
- [21] M. Hoener, L. Fang, O. Kornilov, O. Gessner, S. T. Pratt, M. Gühr, E. P. Kanter, C. Blaga, C. Bostedt, J. D. Bozek, P. H. Bucksbaum, C. Buth, M. Chen, R. Coffee, J. Cryan, L. DiMauro, M. Glowonia, E. Hosler, E. Kukk, S. R. Leone, B. McFarland, M. Messerschmidt, B. Murphy, V. Petrovic, D. Rolles and N. Berrah, *Phys. Rev. Lett.* **104**, 253002 (2010).
- [22] J. P. Cryan, J. M. Glowonia, J. Andreasson, A. Belkacem, N. Berrah, C. I. Blaga, C. Bostedt, J. Bozek, C. Buth, L. F. DiMauro, L. Fang, O. Gessner, M. Guehr, J. Hajdu, M. P. Hertlein, M. Hoener, O. Kornilov, J. P. Marangos, A. M. March, B. K. McFarland, H. Merdji, V. S. Petrović, C. Raman, D. Ray, D. Reis, F. Tarantelli, M. Trigo, J. L. White, W. White, L. Young, P. H. Bucksbaum, and R. N. Coffee, *Phys. Rev. Lett.* **105**, 083005 (2010).
- [23] G. Doumy, C. Roedig, S.-K. Son, C. I. Blaga, A. D. DiChiara, R. Santra, N. Berrah, C. Bostedt, J. D. Bozek, P. H. Bucksbaum, J. P. Cryan, L. Fang, S. Ghimire, J. M. Glowonia, M. Hoener, E. P. Kanter, B. Krässig, M. Kuebel, M. Messerschmidt, G. G. Paulus, D. A. Reis, N. Rohringer, L. Young, P. Agostini and L. F. DiMauro, *Phys. Rev. Lett.* **106**, 083002 (2011).
- [24] H. Thomas, A. Helal, K. Hoffmann, N. Kandadai, J. Keto, J. Andreasson, B. Iwan, M. Seibert, N. Timneanu,

- J. Hajdu, M. Adolph, T. Gorkhover, D. Rupp, S. Schorb, T. Möller, G. Doumy, L. F. DiMauro, M. Hoener, B. Murphy, N. Berrah, M. Messerschmidt, J. Bozek, C. Bostedt and T. Ditmire, *Phys. Rev. Lett.* **108**, 133401 (2012).
- [25] N. Rohringer *et al.*, *Nat. (London)* **481**, 488 (2012).
- [26] B. Rudek *et al.*, *Nat. Photon.* **6**, 858 (2012).
- [27] S. M. Vinko *et al.*, *Nat. (London)* **482**, 59 (2012).
- [28] H. Fukuzawa *et al.*, *Phys. Rev. Lett.* **110**, 173005 (2013); H. Fukuzawa *et al.*, *Phys. Rev. Lett.* **111**, 043001 (2013).
- [29] N. Rohringer and R. Santra, *Phys. Rev. A* **76**, 033416 (2007).
- [30] O. Ciricosta, H.-K. Chung, R. W. Lee and J. S. Wark, *Hi. Ene. Dens. Phys.* **7**, 111 (2011).
- [31] W.-J. Xiang, C. Gao, Y.-S. Fu, J.-L. Zeng and J.-M. Yuan, *Phys. Rev. A* **86**, 061401(R) (2012).
- [32] R. Höppner, Eugenio Roldán, and G. J. de Valcárcel, *Am. J. Phys.* **80**, 882 (2012).
- [33] R. Bonifacio, C. Pellegrini and L. M. Narducci, *Opt. Commun.* **50**, 373 (1984).
- [34] P. Emma, K. Bane, M. Cornacchia, Z. Huang, H. Schlarb, G. Stupakov, and D. Walz, *Phys. Rev. Lett.* **92**, 074801 (2004).
- [35] Y. Ding, A. Brachmann, F.-J. Decker, D. Dowell, P. Emma, J. Frisch, S. Gilevich, G. Hays, Ph. Hering, Z. Huang, R. Iverson, H. Loos, A. Miahnahri, H.-D. Nuhn, D. Ratner, J. Turner, J. Welch, W. White, and J. Wu, *Phys. Rev. Lett.* **102**, 254801 (2009).
- [36] N. R. Thompson and B. W. J. McNeil, *Phys. Rev. Lett.* **100**, 203901 (2008).
- [37] Y. Wang *et al.*, *Nat. Photon.* **2**, 94 (2008).
- [38] J. Zhao *et al.*, *Opt. Express* **16**, 3546 (2008).
- [39] K. Lan, E. Fill, and J. Meyer-Ter-Vehn, *Laser Part. Beams* **22**, 261 (2004).
- [40] S. Jacquemot, K. T. Phuoc, A. Rousse, and S. Sebban, *X-ray Lasers 2006* (Springer, New York, 2007).
- [41] N. Rohringer and R. London, *Phys. Rev. A* **80**, 013809 (2009).
- [42] S. Ackermann *et al.*, *Phys. Rev. Lett.* **111**, 114801 (2013).
- [43] K. C. Kulander, *Phys. Rev. A* **35**, 445 (1987).
- [44] M. Lewenstein, P. Balcou, M. Y. Ivanov, A. L’Huillier and P. B. Corkum, *Phys. Rev. A* **49**, 2117 (1993).
- [45] M. Protopapas, C. H. Keitel and P. L. Knight, *Rep. Prog. Phys.* **60**, 389 (1997).
- [46] S. Patchkovskii, Z.-X. Zhao and T. Brabec and D. M. Villeneuve, *Phys. Rev. Lett.* **97**, 123003 (2006).
- [47] J. Zhao and Z.-X. Zhao, *Phys. Rev. A* **78**, 053414 (2008).
- [48] B. Zhang, J.-M. Yuan and Z.-X. Zhao, *Phys. Rev. Lett.* **111**, 163001 (2013).
- [49] H.-P. Breuer and F. Petruccione, *The theory of open quantum systems*, (Oxford University Press 2002).
- [50] B. R. Mollow, *Phys. Rev. A* **12**, 1919 (1975).
- [51] R. Brewer and E. L. Hahn, *Phys. Rev. A* **11**, 1641 (1975).
- [52] R. Dum, P. Zoller and H. Ritsch, *Phys. Rev. A* **45**, 4879 (1992).
- [53] P. Marte, R. Dum, R. Taieb and P. Zoller, *Phys. Rev. A* **47**, 1378 (1993).
- [54] X.-M. Hu and J.-P. Zhang, *J. Phys. B* **37**, 345 (2004).
- [55] M. Lax, *Phys. Rev.* **129**, 2342 (1963).
- [56] J. H. Eberly, C. V. Kunasz and K. Wodkiewicz, *J. Phys. B* **13**, 217 (1980).
- [57] M. Florjanczyk, K. Rzazewski and J. Zakrzewski, *Phys. Rev. A* **31**, 1558 (1985).
- [58] M. Wilkens and K. Rzazewski, *Phys. Rev. A* **40**, 3164 (1989).
- [59] R. J. Glauber, *In quantum optics and electronics*, (Gordon, and Breach, New York, 1965).
- [60] Y.-Q. Li, J.-H. Wu, Y. Hou and J.-M. Yuan, *J. Phys. B* **41**, 145002 (2008).
- [61] C. Gao, J.-L. Zeng, Y.-Q. Li, F.-T. Jin, J.-M. Yuan, *Hi. Ene. Dens. Phys.* **9**, 583 (2013).
- [62] C. Gao, F.-T. Jin, J.-L. Zeng and J.-M. Yuan, *New J. Phys.* **15**, 015022 (2013).
- [63] J.-L. Zeng, P.-F. Liu, W.-J. Xiang, J.-M. Yuan, *Phys. Rev. A* **87**, 033419 (2013).
- [64] S. Palaniyappan, *et al.*, *Phys. Rev. Lett.* **94**, 243003 (2005).
- [65] W. Ackermann, *et al.*, *Nat. Photon.* **1**, 336 (2007).
- [66] A. A. Sorokin, *et al.*, *Phys. Rev. Lett.* **99**, 213002 (2007).
- [67] Y.-P. Liu, J.-L. Zeng and J.-M. Yuan, *J. Phys. B: At. Mol. Opt. Phys.* **46**, 145002 (2013).
- [68] M. Drescher, M. Hentschel, R. Kienberger, M. Uiberacker, V. Yakovlev, A. Scrinzi, Th. Westerwalbesloh, U. Kleineberg, U. Heinzmann and F. Krausz, *Nat. (London)* **419**, 803 (2002).